HHS Public Access

Author manuscript

*Dev Cell*. Author manuscript; available in PMC 2018 June 05.

Published in final edited form as:

*Dev Cell*. 2017 June 05; 41(5): 481–495.e5. doi:10.1016/j.devcel.2017.05.002.

# Llgl1 connects cell polarity with cell-cell adhesion in embryonic neural stem cells

**Yves Jossin**[1,5,*,#], **Minhui Lee**[2,3,*], **Olga Klezovitch**[2,*], **Elif Kon**[5], **Alexia Cossard**[5], **Wen-Hui Lien**[2,3,6], **Tania E. Fernandez**[2], **Jonathan A. Cooper**[1,3], and **Valera Vasioukhin**[2,3,4,#,&]

[1]Division of Basic Sciences, Fred Hutchinson Cancer Research Center, WA 98109, USA

[2]Division of Human Biology, Fred Hutchinson Cancer Research Center, WA 98109, USA

[3]Molecular and Cellular Biology Program, University of Washington, Seattle, WA 98195, USA

[4]Department of Pathology and Institute for Stem Cell and Regenerative Medicine, University of Washington, Seattle, WA 98195, USA

## Abstract

Malformations of cerebral cortex (MCC) are devastating developmental disorders. We report here that mice with embryonic neural stem cell-specific deletion of *Llgl1 (Nestin-Cre/Llgl1$^{fl/fl}$)*, a mammalian ortholog of Drosophila cell polarity gene *lgl*, exhibit MCC resembling severe periventricular heterotopia (PH). Immunohistochemical analyses and live cortical imaging of PH formation revealed that disruption of apical junctional complexes (AJCs) was responsible for PH in *Nestin-Cre/Llgl1$^{fl/fl}$* brains. While it is well known that cell polarity proteins govern the formation of AJCs, the exact mechanisms remain unclear. We show that LLGL1 directly binds to and promotes internalization of N-cadherin, and N-cadherin/LLGL1 interaction is inhibited by aPKC-mediated phosphorylation of LLGL1, restricting the accumulation of AJCs to the basolateral-apical boundary. Disruption of N-cadherin-LLGL1 interaction during cortical development in vivo is sufficient for PH. These findings reveal a mechanism responsible for the physical and functional connection between cell polarity and cell-cell adhesion machineries in mammalian cells.

### Keywords

stem cells; cell polarity; cell-cell adhesion; periventricular heterotopia

[#]Correspondence: yves.jossin@uclouvain.be and vvasiouk@fhcrc.org.
[5]Present address: Mammalian development & Cell Biology Unit, Institute of Neuroscience, Université catholique de Louvain, 1200 Brussels, Belgium
[6]Present address: de Duve Institute, Université catholique de Louvain, 1200 Brussels, Belgium
[*]These authors contributed equally to this work
[&]Lead contact

## Introduction

The cerebral cortex is a highly organized brain structure responsible for acquisition and processing of information. During normal cortical development, embryonic neural stem cells (ENSCs) localize to the ventricular surface and organize into a pseudostratified epithelium. These cells are highly polarized with their cell bodies close to the ventricle and their long cytoplasmic processes extending radially away from the ventricle to the pial surface of the cortex. ENSC are connected by prominent cell-cell adhesion structures called apical junctional complexes (AJCs) (Chenn et al., 1998). ENSCs divide asymmetrically in a stem cell-like fashion to replenish themselves and to give rise to immature neurons, which are committed to differentiation. These daughter cells are guided by radial glia processes to migrate away from the ventricular zone and eventually differentiate to become neurons.

Abnormalities in this well-orchestrated process of cerebral cortical development lead to malformations of the cerebral cortex (MCC), which are leading causes of drug-resistant epilepsies, mental retardations and other cognitive disorders (Mochida and Walsh, 2004). Primary cellular defects leading to MCCs range from disorders of cell proliferation and cell survival (genetic microcephaly syndromes) to defects in the integrity of the pial surface (cobblestone dysplasia) (Mochida and Walsh, 2004). A large proportion of MCCs, including classical lissencephaly, lissencephaly with cerebellar hypoplasia, X-linked lissencephaly with abnormal genitalia, subcortical band heterotopia (SBH) and periventricular heterotopia (PH), exhibits abnormal localization of cortical neurons (Francis et al., 2006; Mochida and Walsh, 2004). PH is characterized by ectopic deposition of neurons at the lateral ventricle, which is distinct from SBH displaying ectopic layer of neurons separated from lateral ventricle by a layer of white matter.

While the dynamics and mechanisms of PH are not completely understood, it is believed that impaired migration from the ventricular zone, abnormal proliferation and differentiation, or disruption of the integrity of the neuroepithelium are responsible for this MCC (Lian and Sheen, 2015). Inactivating mutations in human Filamin A (*FLNA*), a large actin-binding protein, are responsible for X-linked bilateral PH in females suffering from epilepsy (Fox et al., 1998). FLNA is responsible for cross-linking cortical actin into a three-dimensional structure and connecting the actin cytoskeleton to the plasma membrane. Both functions are critical for changes in cell shape, cell adhesion and migration (Feng and Walsh, 2004). A microcephaly-associated variant of PH is caused by mutations in ARFGEF2 (Sheen et al., 2004). ARFGEF2 is required for vesicle trafficking from the trans-Golgi network and is necessary for proper membrane delivery of E-cadherin/β-catenin components of the junctional complex in MDCK cells (Sheen et al., 2004). In addition, mutations in genes encoding the receptor-ligand cadherin pair DCHS1 and FAT4 results in abnormal ENSCs accumulation resulting in PH (Cappello et al., 2013).

To explore the role of cell polarity mechanisms in mammalian brain development, we examined the functional significance of the cell polarity protein Lethal giant larvae (Lgl). Lgl is an evolutionarily-conserved WD40 domain-containing protein that plays a critical role in the maintenance of cell polarity downstream from the Par3/Par6/aPKC cell polarity complex and Disheveled, an essential mediator of Wnt signaling (Betschinger et al., 2003;

Dollar et al., 2005). Studies in Drosophila revealed that Lgl regulates cell polarity by maintaining the identity of the basal and lateral membrane domain by counteracting the activity of the Par3/Par6/aPKC and Crumbs/Stardust-Patj protein complexes responsible for maintenance of the apical membrane domain (Tanentzapf and Tepass, 2003; Yamanaka et al., 2003). When activated by Cdc42, aPKC phosphorylates and inactivates Lgl at the apical side, while active non-phosphorylated Lgl at the basolateral side excludes Par6/Par3 from the cellular cortex (Betschinger et al., 2005; Betschinger et al., 2003; Plant et al., 2003).

Mammalian genomes contain two Lgl homologs, *Llgl1* and *Llgl2* (Sripathy et al., 2011; Vasioukhin, 2006). *Llgl1*$^{-/-}$ mice display severe brain disorganization and hemorrhagic hydrocephalus leading to neonatal death (Klezovitch et al., 2004). To rescue hydrocephalus and analyze the role of *Llgl1* in the adult brain, we used conditional knockout approach deleting *Llgl1* in ENSCs. The mutant mice show symptoms of epilepsy and their brains display ectopic deposition of neurons at the ventricular surface, which resembles severe cases of PH. Analyses of *Llgl1* cKO brains reveal decreased size of the AJCs in ENSCs leading to focal disruption of neuroepithelium, formation of neuroepithelial rosettes and internalization of ENSCs into the developing cortex. Internalized *Llgl1* cKO ENSCs produce neurons ectopically toward the ventricle as well as normally, toward the cortical plate. Mechanistically, we demonstrate that Llgl1 directly binds to N-cadherin and this interaction is negatively regulated by aPKC-mediated phosphorylation of Llgl1. We show that Llgl1 is necessary to stabilize N-cadherin in AJCs, which are required for structural integrity of the neuroepithelium. These findings link apical-basal cell polarity with properly localized formation of AJCs responsible for strong cell-cell adhesion between ENSCs.

## Results

### Ablation of *Llgl1* in ENSCs results in severe brain malformation

To generate mice with a deletion of *Llgl1* in ENSCs at the beginning of neurogenesis, mice with a conditional *Llgl1* allele (*Llgl1*$^{loxP/loxP}$) (Klezovitch et al., 2004) were crossed with mice carrying a Nestin promoter-driven Cre recombinase (*Nestin-Cre*$^{+/-}$), which is expressed in central nervous system (CNS) ENSCs starting at embryonic day 10.5 (E10.5) (Graus-Porta et al., 2001). Western blot analysis of total brain proteins revealed a gradual decrease in the levels of LLGL1 starting at day E12.5 of development (Figure 1A). Levels of ENSC marker Nestin were gradually increased and the levels of differentiated neuronal marker neurofilament were modestly decreased in postnatal *Llgl1* cKO brains (Figure 1A, B).

At birth, CNS-specific *Llgl1* cKO mice were indistinguishable from their heterozygous and wild-type littermates. Although growth of mutant pups was delayed, their brains were approximately normal size (Figure 1C–D). *Llgl1* cKO adult mice exhibited sporadic seizures associated with falls and convulsions (Videos S1–4). Histological analysis of *Llgl1* cKO brains revealed completely penetrant disorganization of cerebral cortexes where an ectopic second layer of gray matter was formed between the white matter and the lateral ventricle (Figure 1E′, 1F′, 1G′, 1I′ and 1J′, arrows). The hippocampus in the *Llgl1* cKO brains was also severely disorganized and only rudimentary in size with the CA1-CA3 fields being especially affected (Figure 1G′, H′).

### Periventricular heterotopia in *Llgl1* cKO brains

To identify the cells forming the ectopic layer of gray matter in the cerebral cortex of *Llgl1* cKO brains, we performed immunostainings with cell type-specific markers, NeuroN, a marker of differentiated neurons, and GFAP, a marker of astrocytes. In 2 month-old wild-type mice, NeuroN$^+$ cells were localized to the cortical plate above GFAP$^+$ astrocytes, which lined the corpus callosum and the axonal tracts in the white matter (Figure 2A). A similar NeuroN+ cortical plate was located above GFAP+ astrocytes in *Llgl1* cKO brains, but the ectopic gray matter also contained predominantly NeuroN+ cells and few GFAP+ astrocytes (Figure 2A′). Thus, we conclude that the ectopic gray matter in *Llgl1* cKO brains is comprised of differentiated neurons.

To determine the developmental origin of the ectopic neurons, we performed additional cell-type specific stainings and bromodeoxyuridine (BrdU) birthdating experiments. The *Llgl1* cKO cortical plate showed the normal features of cortical stratification, with early-born neurons, labeled with BrdU on day E13.5 and expressing TBR1 (layer VI) and CTIP2 (layer V), positioned below later born neurons, labeled with BrdU on day E16.5 and expressing BRN1 (layers II–IV) and CUX1 (layers II–IV) (Figure 2B–G′, Figure S1A). However, the ectopically localized NeuN+ neurons expressed BRN1 and CUX1, with only few cells expressing TBR1 and CTIP2, and were prominently labeled with BrdU on day E16.5 but less on E13.5, implying that the majority of these neurons were born during late neurogenesis (Figure 2C–2G′, Figure S1B). Remarkably, new cell birth could still be detected in *Llgl1* cKO cortexes at E18.5, when cortical neurogenesis was almost completed in wild-type brains (Figure 2H–H′). Overall, we conclude that the ectopic gray matter in *Llgl1* cKO brains is comprised of neurons that are mostly born during late stages of neurogenesis and express appropriate stage-specific markers, while the layering of the primary cortical plate is not grossly altered. The MCC in *Llgl1* cKO brains is strikingly similar to MCC in human patients suffering from severe PH, which is characterized by the formation of ectopic nodules or a band of neurons along the lateral ventricle. Remarkably, sporadic seizures are one of the main symptoms of patients with PH (Lu and Sheen, 2005). We conclude that CNS-specific *Llgl1* cKO mice develop prominent MCC which is consistent with PH.

### Mislocalization of ENSCs prior to the formation of second cortical neuronal layer in *Llgl1* cKO brains

To determine the cellular mechanisms responsible for cortical malformation in *Lgl1*$^{-/-}$ brains, we analyzed mutant mice at various times during embryonic development (Figure 3). During normal neurogenesis, self-renewing ENSCs (Nestin+/Pax6+/Tbr2-) localize at the surface of the lateral ventricles (Figure 3A, 3F). ENSCs are highly polarized cells with apical membrane domains facing the ventricle (Crb3+) and long glial processes (RC2+) pointing away from the ventricle toward the developing cortex (Figure 3E). Endogenous LLGL1 is prominently expressed and is localized to the lateral membrane domain and the cytoplasm of ENSCs (Figure S2). During neurogenesis, ENSCs divide asymmetrically to self-renew and to generate subventricular zone (SVZ) progenitors (Nestin-/Pax6-/Tbr2+), which are committed to differentiation. SVZ progenitors do not maintain AJCs and do not incorporate into the ventricular wall. These cells reside in a position basal to the ENSCs,

somewhat removed from the ventricles (Figure 3F, G, green). SVZ progenitors divide to generate post-mitotic, immature neurons which use radial glial processes of neural progenitors to migrate toward the developing cortical plate, where they differentiate into neurons (β-Tubulin III+) (Figure 3B).

To analyze the dynamics of cortical malformation in *Lgl1*$^{-/-}$ brains we first used immunostaining with anti-Nestin and anti-β-Tubulin III antibodies. While Nestin+ ENSCs were located normally at the edge of the ventricle in E12.5 *Llgl1* cKO brains, by E14.5 the ENSC layer was discontinuous and small β-Tubulin III+ neuronal nodules formed at the ventricular surface (Figure 3A′, white arrowhead). The total length of the neurogenic region was also noticeably increased in mutant brains, suggesting a significant increase in area of the neurogenic surface (Figure 3A′). By E17.5, the ENSC niche disintegrated into distinct foci surrounded by differentiating neurons (Figure 3B′, C′, arrows). Nestin+ cells had largely disappeared from normal cortex after birth, but were still detected in mutant cortex until P5 forming a discontinuous layer in the middle of the developing cortex (Figure 3D′, arrow). At the cellular level, wild-type ENSCs display their apical membrane domains facing the ventricle (Crb3+) and radial glial processes extending toward the cortical plate (Figure 3E). In contrast, *Llgl1* cKO ENSCs that were mislocalized to the inside of the developing cortices contained apical membrane domains in the middle of Nestin+ cell masses and extended radial glial processes towards the ventricle as well as towards the developing cortical plate (Figure 3E–E′). Nestin+ cells in the middle of *Llgl1* cKO cortices were comprised of both ENSCs (Pax6+) and differentiating SVZ progenitors (Tbr2+) (Figure 3F–G′). This organization and cell-type specificity of Nestin+ cells inside the *Llgl1* cKO cortices suggested that ENSCs were internalized in E17.5 *Llgl1* cKO brains.

## Absence of LLGL1 perturbs cell migration during development

To visualize the formation of PH in *Llgl1* cKO cortices, we used time-lapse video microscopy with organotypic embryonic brain slices. For this purpose, we first utilized in utero electroporation procedure to introduce a plasmid encoding nuclear GFP into E12.5 ENSCs (Tabata and Nakajima, 2001). One day later, we isolated the brains and prepared cortical slices and genotyped the embryos. GFP expressing slices from control and *Llgl1* cKO cortices were identified and imaged for 12–16 hours. Imaging cortical slices from control embryos revealed interkinetic nuclear movements of ENSCs (Video S5). During this process ENSC nuclei move from a basal position to the apical surface where the cells divide mitotically and afterwards their nuclei again migrate basally away from the ventricular surface (Spear and Erickson, 2012). (Figure 4A, Video S5). In contrast, in *Llgl1* cKO cortical slices, ENSC nuclei did not migrate towards the apical surface and divided at a more basal position. In addition, daughter cells exhibited random movements with a tendency to move towards the apical surface (Figure 4A, Video S5).

When ENSCs were in utero electroporated with GFP plasmid at E14.5 and then imaged two days later at E16.5, *Llgl1* cKO ENSCs formed rosette-like structures (Figure 4B, Video S6). These are likely the origin of the rosettes detected in fixed sections at E17.5 (Figure 3F′).

Cortical electroporation is a highly invasive procedure which, while relatively well tolerated in normal cortexes, may potentially accelerate disorganization in *Llgl1* cKO brains.

Therefore, we decided to label and image ENSCs using less invasive technique. We labeled ENSCs by injecting membrane-permeable Cell Tracker Green into E13.5 brain ventricles. We then generated cortical slices and imaged them for 12–16 hours. While imaging of cells labeled with cell tracker dye provided less contrast than imaging of cells expressing nuclear GFP, this approach enabled us to commence imaging of cortexes before *Llgl1* cKO brains are overtly disorganized. Imaging cortical slices from control animals reveal ENSCs close to the ventricular surface at the beginning of the time lapse with cell bodies moving toward more basal position (Video S7). In contrast, in *Llgl1* cKO cortical slices, we observed focal disruption of the ventricular wall and prominent movement of cells into the ventricular space (Video S7).

## Disruption of ventricular wall integrity results in internalization of ENSCs in *Llgl1 cKO* brains

To reveal the mechanisms responsible for internalization of *Llgl1* cKO ENSCs, we analyzed developing cortices at E14.5, before fragmentation and mislocalization of ENSC niches occurs. In wild-type brains the ventricular surface is lined by the apical membrane domains of ENSCs. N-cadherin based cell-cell adhesion structures called AJCs separate the apical and basolateral membrane domains of ENSCs. Reinforced by the actin cytoskeleton, AJCs connect ENSCs to each other at the surface of the ventricle to form a strong net that keeps ENSCs inside the cortex and prevents their emergence on the ventricular surface (Kadowaki et al., 2007). Interestingly, immunostaining for the AJC markers N-cadherin and α-catenin revealed focal disruption of AJCs in *Llgl1* cKO ENSCs at E14.5, the time point immediately before the disruption of ENSC niches and mislocalization of ENSCs takes place (Figures 4C–D′, S3). Short fragments of E14.5 *Llgl1* cKO cortices displayed complete loss of AJCs (Figures 4D–D′, S3B–B″, arrowheads). Cells in these areas protruded into the ventricular space (Figures 4D′, S3B–B″), resembling focal protrusion and movement of ventricular zone cells into the ventricular space observed by live imaging (Video S7). These protrusions were still populated by Nestin+ ENSCs (Figure S3E–G). Localized disruption of AJCs in *Llgl1* cKO brain may be responsible for focal protrusion and expansion of nonpolarized cells on the ventricular surface in these cortical areas. As these nonpolarized cells continue to expand at the ventricular surface later in development, fragments of the neuroepithelium containing polarized ENSCs maintaining residual AJCs can become completely engulfed by their nonpolarized neighbors and internalized into the cortex. Indeed, later in development at E17.5, the apical membrane domains and AJCs localize to the center of rosettes in the middle of developing *Llgl1* cKO cortices (Figures 4E–E′, S3C–D″). These findings are consistent with a model where focal disruption of AJCs in *Llgl1* cKO cortices is responsible for protrusion of ENSCs into the ventricular space, formation of neuroepithelial rosettes and internalization of ENSCs (Figure 4F).

## LLGL1 is necessary for the maintenance of prominent AJCs in ENSCs

Since immunostaining for markers of AJCs of ENSCs demonstrated focal loss of staining in E14.5 *Llgl1* cKO cortexes (Figure 4D–D′), we analyzed AJCs using electron microscopy. As expected, electron dense AJCs were found at the interface between apical and lateral membrane domains of ENSCs in control embryos (Figure 5A–A′, arrows). AJCs were present in the regions containing polarized ENSCs in *Llgl1* cKO cortexes (Figure 5B–B′,

arrowheads). However, these structures were absent from cells that protruded into the ventricle (Figure 5C–C′). Quantitation of the lengths of AJCs revealed significant decrease in the size of AJCs in E14.5 *Llgl1* cKO ENSCs in the areas that maintained cell polarity (Figure 5D, *Llgl1* cKO P). These findings indicate overall decrease in sizes and focal loss of AJCs in E14.5 *Llgl1* cKO ENSCs, which is likely responsible for the focal loss of ventricular wall integrity and protrusion of cells into the ventricular space.

AJCs in ENSCs are made primarily by the adherens junctions containing N-cadherin (Chenn et al., 1998). In agreement with electron microscopy, high magnification confocal microscope analysis of N-cadherin staining revealed prominent disorganization of N-cadherin-containing AJCs in E14.5 *Llgl1* cKO cortexes, even in the areas that maintained the integrity of the ventricular wall (Figure S4). Abnormal junctions may be the result from decreased levels of adherens junction proteins N-cadherin, α- and β-catenins, failure of cadherin-catenin protein complex formation, failure of cadherin-catenin complex delivery and retention at the plasma membrane, or failure of clustering and stabilization of adhesion complexes by association with the actin cytoskeleton (Yap et al., 2015). We found no differences in the total levels of cadherin and catenin proteins or in the cadherin-catenin complex formation in E14.5 *Llgl1* cKO ENSCs (Figure 5E). The levels of cell surface N-cadherin were not decreased, but increased in *Llgl1* cKO ENSCs and this phenotype was rescued by re-expression of LLGL1 (Figure 5F–G). Endocytosis experiments revealed prominent decrease in internalization of N-cadherin in *Llgl1* cKO ENSCs (Figure 5H), while overall rates of N-cadherin protein synthesis and degradation were unchanged (Figure 5I). These data and the decrease in the length and focal disruption of AJCs in *Llgl1* cKO ENSCs which was observed by EM (Figure 5A–D), suggest the defects in polarized clustering of cadherin-catenin proteins and their assembly into the AJCs in Llgl1$^{-/-}$ cells.

## Physical interaction between LLGL1 and N-Cadherin

To understand how LLGL1 regulates formation of AJCs, we decided to analyze whether LLGL1 physically interacts with cadherin-catenin proteins. Indeed, co-immunoprecipitation experiments revealed association between endogenous LLGL1 and N-cadherin in E14.5 brains (Figure 6A–B). In pull-down assays with purified β-catenin or cytoplasmic domain of N-cadherin, LLGL1 preferentially bound to N-cadherin (Figure 6C). LLGL1 function is negatively regulated by atypical protein kinase C (aPKC)-mediated phosphorylation of five evolutionary conserved serines in the middle of the protein (Plant et al., 2003), which results in interaction between the N- and C-terminal domains of Lgl and release of cortical Lgl into the cytoplasm (Betschinger et al., 2005; Prehoda, 2009). To determine whether interaction between LLGL1 and N-cadherin is regulated by phosphorylation at aPKC target sites, we generated expression constructs encoding wild-type, phospho-mimicking 5SD and unable to be phosphorylated 5SA mutant of LLGL1. Both wild-type and 5SA mutant of LLGL1 interacted with cytosolic fragment of N-cadherin (Figures 6D, S5A). In contrast, 5SD mutant LLGL1 displayed weak binding to N-cadherin (Figure S5A). Co-expression of constitutively-active aPKC decreased the binding between wild-type LLGL1 and N-cadherin, while interaction between 5SA mutant LLGL1 and N-cadherin was not affected (Figure 6D). These data indicate that aPKC-mediated phosphorylation inhibits LLGL1-N-cadherin interaction.

To map the domains of LLGL1 and N-cadherin responsible for interaction, we generated and performed immunoprecipitation experiments with various truncated fragments of both LLGL1 and N-cadherin (Figure 6E–H′). The fragments containing C-terminal WD14 domain of LLGL1 and, to a lesser degree, fragment containing WD10 domain were responsible for interaction with N-cadherin (Figures 6E–F′). Conversely, the β-catenin-binding region and the adjacent C-terminal portion of N-cadherin were necessary for interaction with LLGL1 (Figure 6G–H′). Since we found an overlap between β-catenin and LLGL1-binding regions on N-cadherin, we analyzed whether binding of N-cadherin to LLGL1 and β-catenin is mutually exclusive. Co-immunoprecipitation experiments demonstrated that LLGL1, N-cadherin and β-catenin form tripartite complex and N-cadherin is necessary for interaction between LLGL1 and β-catenin (Figure S5B). To determine whether LLGL1-N-cadherin interaction is direct, we performed pull-down experiments with proteins purified from bacteria. C-terminal WD14 domain-containing fragment, but not the fragment containing aPKC phosphorylation sites of LLGL1 directly bound cytoplasmic domain of N-cadherin, indicating that LLGL1-N-cadherin interaction is direct (Figure 6I). Finally, we found that C-terminal truncation deleting both N-cadherin-binding sites of LLGL1 (WD14 and WD10) was necessary to prevent interaction between LLGL1 and N-cadherin (Figure S5C).

## Disruption of LLGL1-N-cadherin interaction in developing brain in vivo results in periventricular heterotopia

To determine the significance of LLGL1-N-cadherin interaction, we decided to disrupt it using a dominant-negative approach. We hypothesized that overexpression of directly interacting with N-cadherin C-terminal WD14 domain of LLGL1 would compete with full-length endogenous LLGL1 for binding to N-cadherin. Indeed, overexpression of a protein containing triple repeat of C-terminal WD14 domain of LLGL1 linked to GFP (3xLLGL1#9-GFP) significantly decreased, but not completely abolished, interaction between LLGL1 and N-cadherin (Figure 7A).

To determine the functional significance of interaction between LLGL1 and N-cadherin in developing brain in vivo, we decided to use in utero electroporation technique, which is capable to deliver DNA expression constructs into E15.5 cortexes (Saito, 2006). Since these experiments significantly differ from genetic inactivation of *Llgl1* at E10.5 by *Nestin-Cre*, we first analyzed whether loss of endogenous Llgl1 in the framework of such an experiment would generate neuronal heterotopia resembling the cortical phenotype in *Llgl1* cKO embryos. As expected, in utero electroporation of E15.5 cortexes with plasmids expressing non-targeting shRNA did not result in the development of heterotopia (Figure 7B). In contrast, in utero electroporation of the plasmid expressing sh-Llgl1 resulted in the development of focal neuronal heterotopia in all electroporated cortexes (Figures 7B, S6) white arrow). This phenotype was rescued by simultaneous expression of full-length, but not C-terminally truncated, unable to bind to N-cadherin human LLGL1 (Figure 7B). Since aPKC-mediated phosphorylation decreases the binding between N-cadherin and LLGL1, we analyzed whether activation and plasma membrane targeting of aPKC can mimic shLlgl1 phenotype. While expression of activation loop constitutively-active aPKC (CA-aPKC) or its binding partner Par3 alone did not cause heterotopia (data not shown), coexpression of CA-

aPKC and Par3 resulted in completely penetrant neuronal heterotopia phenotype (Figure 7C). Importantly, this phenotype was partially rescued (3 out of 5) by simultaneous expression of non-phosphorylatable 5SA LLGL1 (Figure 7C).

Since expression of 3xLLGL1#9-GFP weakens interaction between LLGL1 and N-cadherin, we also analyzed the consequences of disruption of endogenous LLGL1-N-cadherin binding using in utero electroporation. Expression of 3xLLGL1#9-GFP protein resulted in the development of a partially penetrant neuronal heterotopia phenotype (4 out of 7 brains) (Figure 7C). Therefore, we concluded that direct interaction between LLGL1 and N-cadherin is necessary for stabilization of N-cadherin at the AJCs.

## Discussion

Malformation of cerebral cortex is a constellation of devastating human brain disorders that account for a significant proportion of epilepsy and mental retardation (Mochida and Walsh, 2004). The dynamics and molecular mechanisms that underlie human MCCs have remained poorly understood. Studies of human brain tissues from patients with MCC associated with PH have led to the general conclusion that ectopic deposition of neurons results from defects in neuronal migration (Mochida and Walsh, 2004) or loss of neuroependymal integrity (Ferland et al., 2009). The integrity of the ventricular surface during development is maintained by the AJCs of ENSCs. Disruption of AJCs by genetic or shRNA-mediated inactivation of RhoA, N-cadherin, α- or β-catenin results in profound defects in proliferation, differentiation and delamination of ENSCs (Cappello et al., 2006; Cappello et al., 2012; Junghans et al., 2005; Kadowaki et al., 2007; Katayama et al., 2011; Kim et al., 2010; Lien et al., 2006; Machon et al., 2003; Zechner et al., 2003). Loss of AJCs during neurogenesis in RhoA or αE-catenin mutants or in embryos with shRNA-mediated knockdown of Filamin A results in formation of ectopically positioned neuronal masses resembling PH (Cappello et al., 2012; Carabalona et al., 2012; Schmid et al., 2014). *ARFGEF2*, a gene previously implicated in PH in human patients, may also be responsible for the maintenance of AJCs due to its involvement in the membrane delivery of N-cadherin/β-catenin complexes, which is necessary for proper cell-cell adhesion (Sheen et al., 2004).

We found that deletion of *Llgl1* during cortical neurogenesis results in the development of PH. Presently, the phenotypes of humans with mutations in *LLGL1* are not known and it is not clear if some patients with neuronal heterotopias have mutations in this gene. We analyzed the cellular mechanisms responsible for the formation of PH in *Llgl1* cKO mice using variety of techniques including live imaging of developing *Llgl1* cKO cortexes. To our knowledge, this is the first imaging of PH formation in live cortical tissue. We found that LLGL1 is necessary for the maintenance of prominent AJCs in ENSCs and that ablation of *Llgl1* results in focal disruption of the integrity of ventricular wall and internalization of ENSCs which maintain residual cell polarity and AJCs. Internalized ENSCs form neuroepithelial rosette-like structures in the middle of the developing cortex and send out differentiating neurons to both normal cortical plate and ventricular surface, effectively creating an ectopic layer of neurons at the ventricular surface of *Llgl1* cKO cortices.

LLGL1 is an apical-basal cell polarity protein; however, we found that maintenance of AJCs is the critical function of LLGL1 in mammalian brain. Cell polarity pathways may be intimately interconnected with cell-cell adhesion complexes. AJC represents the structure that physically separates the apical and basolateral membrane domains. Basolateral polarity complexes Lgl/Dlg/Scribble are required for AJC formation in epithelial cells (Bilder et al., 2003; Laprise et al., 2004; Qin et al., 2005; Tanentzapf and Tepass, 2003). We now demonstrate that mammalian LLGL1 is necessary for the maintenance of AJCs and that loss of adhesion is responsible for PH in *Llgl1* cKO brains. What is the mechanism responsible for LLGL1 function in AJC maintenance? We found that LLGL1 directly interacts with N-cadherin and this binding is negatively regulated by aPKC-mediated phosphorylation. This interaction is important for LLGL1 function in brain development, because targeted disruption of this interaction in vivo is sufficient for neuronal heterotopia. We propose that the direct interaction of LLGL1 with N-cadherin contributes to the strengthening of AJCs and helps to maintain the integrity of the ventricular wall during embryonic brain development. Since interaction between LLGL1 and N-cadherin is disrupted by aPKC-mediated phosphorylation of LLGL1, and aPKC is concentrated at the AJCs of the ENSCs (Manabe et al., 2002), LLGL1 would not be able to bind N-cadherin at this location. Thus, we propose a following hypothetical model of LLGL1 function (Figure 7D). Since LLGL1 is necessary for internalization of plasma membrane bound N-cadherin, it can differentially regulate N-cadherin internalization, promoting internalization at the lateral membrane domain but failing to do so at the AJCs, where aPKC phosphorylates LLGL1 and prevents LLGL1-N-cadherin interaction (Figure 7D). In this scenario, the local concentration of N-cadherin at the AJCs will increase, while concentration of N-cadherin at the large lateral membrane domain will be kept at the minimum via LLGL1-mediated internalization. If this model is correct, aPKC should be essential for AJC formation, because without aPKC, LLGL1 would promote internalization of N-cadherin at the AJCs and, therefore, destabilize their integrity. Remarkably, in vivo deletion of aPKC lambda in ENSCs results in a complete loss of AJCs, which is in an agreement with this prediction (Imai et al., 2006).

It has been previously reported that LLGL proteins physically interact with Myosin II and that aPKC-mediated phosphorylation disrupts this binding (Dahan et al., 2014; Strand et al., 1995). This functional interaction is important for microridge elongation in developing zebrafish epidermis (Raman et al., 2016). It is possible that LLGL1 links N-cadherin with myosin IIB which can potentially facilitate clustering of cadherins into prominent AJC structures. Indeed, Myosin IIB is colocalized with AJCs and it is critical for AJC maintenance (Ma et al., 2007; Smutny et al., 2010). We analyzed possible role of LLGL1 in linking N-cadherin with myosin IIB; however, we found that overexpressed in HEK293 cells LLGL1 and Myosin IIB compete for rather than facilitate each other interaction with N-cadherin (Figure S6B), indicating that this mechanism of LLGL1 function in AJC formation is not very likely. In addition to the reported here direct interaction between LLGL1 and N-cadherin, LLGL1 may potentially indirectly regulate AJCs via its role in regulation of Par3-aPKC complexes, Rab-mediated endosomal trafficking and/or its role in negative regulation of Notch signaling (Clark et al., 2012; Das et al., 1990; Klezovitch et al., 2004; Yamanaka et al., 2003). Additional research will be necessary to examine the mechanisms of LLGL1 in N-cadherin-mediated cell–cell adhesion.

# STAR★Methods

## Contact for Reagent and Resource Sharing

Further information and requests for reagents may be directed to, and will be fulfilled by, the Lead Contact, Valera Vasioukhin (vvasiouk@fhcrc.org).

## Experimental Model and Subject Details

**Mouse strains and genotyping—**Animal studies were performed in accordance with guidelines of the Animal Care and Use Committee of the Fred Hutchinson Cancer Research Center (FHCRC) and all colonies were maintained following animal research guidelines at FHCRC. Mice with CNS-specific knockout of *Llgl1 (cKO Llgl1)* were obtained by breeding mice carrying conditional *Llgl1* allele (Klezovitch et al., 2004) with *Nestin-Cre* transgenic mice (Graus-Porta et al., 2001; Tronche et al., 1999). $Llgl1^{LoxP/+}/Nestin\text{-}Cre^{+/-}$ males were crossed with $Llgl1^{LoxP/LoxP}$ females. Mice were on C57BL/6J genetic background. Both male and female mice were analyzed and no differences were observed between the sexes.

**In utero electroporation of developing cerebral cortexes—**In utero microinjection and electroporation was performed at E15.5 essentially as described (Tabata and Nakajima, 2001), using timed pregnant CD-1 mice (Charles River Laboratories). In brief, mice were anesthetized and the midline incision the uterine horns were exposed. Plasmid solution was injected into the lateral ventricle using needles for injection that were pulled from Wiretrol II glass capillaries (Drummond Scientific) and calibrated for 1-l injections. DNA solutions were mixed in 10 mM Tris, pH 8.0, with 0.01% Fast Green. The embryo in the uterus was placed between the forceps-type electrodes (Nepagene) with 5 mm pads and electroporated with five 50-ms pulses of 45 V using the ECM830 electroporation system (Harvard Apparatus). The uterine horns were then placed back into the abdominal cavity to continue normal brain development.

**Organotypic slice culture of cerebral cortexes and time-lapse confocal microscopy—**300-m embryonic brain slices were prepared using a vibratome (World Precision Instruments) as described (Jossin et al., 2003). In brief, the whole fetal brain was embedded in 4% low melting agarose (Promega, Madison, WI) prepared in DMEM-Hank's F12 medium with glutamine, glucose, and HEPES and glued on a vibratome support using cyanoacrylate. Slices were cut in the coronal plane. Time-lapse confocal microscopy was performed using an Achroplan × 20/0.50 with a Zeiss LSM 5 Pascal confocal on an Axioskop2 upright microscope. Slices were embedded in a drop of 3% agarose and cultured in a chamber on a heated stage (Warner Instruments) in DMEM-F12 (Invitrogen) supplemented with B27 (Invitrogen) and 10% serum. The medium was preheated at 37 °C and equilibrated with 95% $O_2$ and 5% $CO_2$. The medium was flowed into the chamber at ~5 ml/h. Repetitive acquisitions were performed in laterodorsal regions of the cortex in which 25 successive z optical planes spanning 120 m were acquired. Z-stacks were selected and combined in Zeiss LSM Image Browser. Slight drifts of the slices were corrected using the ImageJ registration tool Turboreg (P. Thévenaz, Biomedical Imaging Group, Swiss Federal Institute of Technology, Lausanne, Switzerland).

**Labeling of ventricular zone neurons with CMFDA compound—**Labeling was performed as previously described (Jossin and Goffinet, 2007). In brief, whole brains from embryos were removed and Cell Tracker Green CMFDA (Molecular Probes C-2925) was injected in the ventricles at a concentration of 5 μM. Brains were then incubated for 15 min at 37°C and sliced at 300 μm. Comparable coronal slices were selected and cultured for time-lapse confocal microscopy.

**Isolation, culture and nucleofection of primary murine ENSCs—**Primary ENSCs for tissue culture experiments were isolated from E11.5 mouse brains by digestion of isolated brains with Accutase for 15 min at room temperature and mechanical disaggregation. Cells were grown on laminin-coated plates in NSC growth media: 100 ml NS-A basal medium, 100 ml DMEM-F12 medium, 2 ml B27, 2 ml N2, 2 ml Pen/Strep, 2 ml L-glutamine, 10 ng/ml mEGF, and 10 ng/ml hFGF2. For plasmid DNA transfection, cells were Amaxa nucleoporated with 5 μg of plasmid DNA in 0.2 mm cuvette (Sigma) using A-033 program and 100 μl of electroporation buffer containing 120 mM $Na_2HPO_4$/$NaH_2PO_4$ pH 7.2, 5 mM NaCl, 5 mM KCl, 20 mM $MgCl_2$, and 0.5 mM reduced glutathione.

**Cell Lines—**HEK293FT cells were obtained from ATCC and used within 10 passages since arrival. Cells were transfected using PEI (Polyethylenimine) with final DNA concentration of 0.8 μg/ml and final PEI concentration 2 μg/ml in total culture media.

## Method Details

**Histology and electron microscopy—**Tissues for histology were fixed in 4% paraformaldehyde, processed and embedded in paraffin. Sections (4μm) were stained with hematoxylin and eosin, examined and photographed using the Nikon TE 200 microscope. For transmission electron microscopy (EM), samples were fixed in 2% glutaraldehyde, 4% formaldehyde in 0.05M sodium cacodylate buffer at 4ºC overnight and processed for Epon embedding. Samples were visualized with a JEOL 1010 microscope.

**Immunofluorescence—**For immunofluorescence staining tissues were fixed in 4% formaldehyde/PBS at 4°C, embedded in paraffin, sectioned and resulting 5 μm sections were deparaffinised, dehydrated, treated with antigen retrieval solution, blocked in Superblock with 5% normal goat serum for 1 h at room temperature, incubated with primary antibodies in block solution with 0.1% Triton X100, washed 4 times for 5 minutes each in PBS, and incubated with immunofluorescently labelled secondary antibodies diluted in Superblock solution with 0.1% Triton X100. For staining on frozen sections, tissues were fixed in 4% formaldehyde/PBS at 4°C, embedded in OCT, and sectioned. Sections were postfixed in 4% formaldehyde for 8 minutes, permeabilized in 0.1% Triton X100 in PBS and stained as described above. Stained slides analysed using the Nikon TE 200 microscope with COOLSNAP HQ digital camera, or using Zeiss LSM 700 Confocal Microscope with ZEN imaging software.

**Antibodies—**Antibodies used: anti-β-Tubulin III (Western Blot (WB): 1:2,000, Immunofluorescence (IF): 1:500), anti-β-Actin (WB; 1:10,000), anti-β-catenin (WB:

1:5,000, IF: 1:1,000), anti-α-Catenin (WB:1:1,000, IF 1:2,000), anti-Nestin (DSHB Rat-401, IF 1:5; ATCC SCRR-1001, WB: 1:1,000, IF: 1:200), anti-BrdU (IF: 1:5), anti-RC2 (IF 1:5), anti-Pax6 (IF: 1:5), anti-N-Cadherin (WB; 1:1,000, IF: 1:100, IP: 0.5 μg), anti-NeuroN (IF: 1:200), anti-GFAP (IF: 1:2,000), anti-Neurofilament (WB: 1:1,000, IF: 1:500), anti-phospho-histone 3 (IF: 1:200), anti-Tbr2 (IF: 1:2,500) and anti-Tbr1 (IF: frozen sections, 1:1,000), anti-Brn1 (IF: 1:500), anti-*Llgl1* (WB: 1:2,000), anti-Crumbs 3 (IF: 1:200), anti-CTIP2 (1:200), anti-CUX1/CDP (1:50). Anti-Llgl1 antibodies were generated in rabbits using GST-Lgl1 fusion containing 356 amino acids (aa) of mouse Llgl1 (aa679-1034, NM_008502) (WB: 1:2,000, IF: 1:5,000). All incubations with primary antibodies were performed overnight at +4°C. All stainings were performed on deparaffinized waxed sections except where indicated otherwise.

**Molecular cloning—**All primers used for cloning can be found in Table S1. Murine LLGL1 was amplified from cDNA using Llgl1 Forward and Llgl1 Reverse primers with Pfu polymerase and cloned into the gateway entry vector pCR8/GW/TOPO vector. Plasmids expressing full-length and cytoplasmic domain of N-cadherin were described in (Jossin and Cooper, 2011). Plasmid expressing full-length β-catenin was described in (Lien et al., 2008). LLGL1 with S to A or S to D mutations of 5 aPKC phosphorylation sites were generated by using Stratagene Quick Change kit and following oligo pairs: Llgl1_StoA F and Llgl1_StoA R; Llgl1_StoD F and Llgl1_StoD R.

Plasmids encoding fragments of Llgl1 were made by TOPO cloning into pCR8/GW/TOPO using DNA fragments generated by PCR amplification with following oligos: Llgl1#2 with oligos LLGL1-#2F and LLGL1-#2R; Llgl1#3 with oligos LLGL1-#2F and LLGL1-#3R; Llgl1#4 with oligos LLGL1-#4F and LLGL1-#4R; Llgl1#5 with oligos LLGL1-#5F and LLGL1-#5R; Llgl1#6 with oligos LLGL1-#6F and LLGL1-#6R; Llgl1#7 with oligos LLGL1-#7F and LLGL1-#7R; Llgl1#8 with oligos LLGL1-#8F and LLGL1-#8R; Llgl1#9 with oligos LLGL1-#9F and Llgl1 Reverse; Llgl1#10 with oligos Llgl1 Forward and LLGL1-#10R; Llgl1#11 with oligos LLGL1-#11F and LLGL1-#11R; Llgl1#12 with oligos LLGL1-#12F and LLGL1-#12R. Plasmids with c-terminal deletions of Llgl1 were made using Q5 mutagenesis of full-length Llgl1 in pDEST27 with following oligos: LLGL1Δ910-1062 with oligos LLGL1Δ910-1062F and LLGL1Δ910-1062R; LLGL1Δ649-1062 with oligos LLGL1Δ910-1062F and LLGL1Δ649-1062R; LLGL1Δ599-1062 with oligos LLGL1Δ910-1062F and LLGL1Δ599-1062R. For expression in bacteria, Llgl1#5 and Llgl1#9 fragments were released from pCR8/GW/TOPO with EcoRI and subcloned into EcoRI site of pMAL-p5X.

Plasmids encoding fragments of N-cadherin were made by TOPO cloning into pCR8/GW/TOPO using DNA fragments generated by PCR amplification with following oligos: N-cadherin cyto #1 with oligos N-cadherin cyto #1F and N-cadherin cyto #1R; N-cadherin cyto #2 with oligos N-cadherin cyto #2F and N-cadherin cyto #2R; N-cadherin cyto #3 with oligos N-cadherin cyto #3F and N-cadherin cyto #3R; N-cadherin cyto #4 with oligos N-cadherin cyto #4F and N-cadherin cyto #4R; N-cadherin cyto #5 with oligos N-cadherin cyto #5F and N-cadherin cyto #5R; N-cadherin cyto #6 with oligos N-cadherin cyto #6F and N-cadherin cyto #6R; N-cadherin cyto #7 with oligos N-cadherin cyto #7F and N-cadherin cyto #4R; N-cadherin cyto #8 with oligos N-cadherin cyto #4F and N-cadherin cyto #6R; N-

cadherin cyto #9 with oligos N-cadherin cyto #4F and N-cadherin cyto #5R; N-cadherin cyto #10 with oligos N-cadherin cyto #5F and N-cadherin cyto #6R; N-cadherin cyto #11 with oligos N-cadherin cyto #11F and N-cadherin cyto #11R; N-cadherin cyto #12 with oligos N-cadherin cyto #5F and N-cadherin cyto #11R; N-cadherin cyto #13 with oligos N-cadherin cyto #11F and N-cadherin cyto #6R.

shCtrl FUGW-H1-GFP was described in (Lien et al., 2008). shLlgl1 was generated by annealing oligos shLlgl1F and shLlgl1R, extending them with T4, cutting with EcoRI +BamHI and cloning into EcoRI+BamHI sites of shCtrl. 3xLLGL1#9-GFP construct was generated by PCR amplification of LLGL1#9 with oligos 3xLLGL1#9-GFPf and 3xLLGL1#9-GFPr, cutting the fragment with EcoRI+MfeI, ligation of fragments to each other, re-cutting again with EcoRI+MfeI, gel purification of 3x fragment and ligation into EcoRI site of pCAG-GFP. LLGL1-GFP was generated by subcloning released by EcoRI digestion full-length Llgl1 from pCR8/GW/TOPO vector into EcoRI site of pCAG-GFP. Human LLGL1-full length construct was generated by PCR amplification of clone 8860300 GB:BC151838 (Open Byosystems) with oligos hLLGL1F and hLLGL1R and TOPO cloning into pCR8/GW/TOPO. Human LLGL1 expression construct was then generated by subcloning of EcoRI fragment containing LLGL1 from pCR8/GW/TOPO to EcoRI site of pCAGIG. Human LLGL1-Δ614-1064 construct was generated by PCR amplification with oligos hLLGL1-Δ614-1064F and hLLGL1-Δ614-1064R and cloning it into EcoRI-EcoRV sites of pCAGIG. PKCzeta was subcloned from PKCzeta T410E into EcoRI site of pCAGIG.

Gateway technology was used to generate GST-(pDEST27) or V5-(pcDNA3.1/nV5-DEST) tagged expression constructs for eukaryotic expression. All constructs were verified by sequencing.

**Immunoprecipitation and Western blot analysis—**Western blot analyses and immunoprecipitations were carried out according to standard protocols (Harlow and Lane, 1999). Steady-state cell surface levels of N-cadherin on isolated primary ENSCs were determined by cell-surface biotinylation followed by pull-down with streptavidin beads and Western blotting with anti-N-cadherin antibodies (Teng et al., 2005). ENSCs for these experiments were isolated from whole brain tissue by treatment with Trypsin in the presence of $Ca^{2+}$ followed by gentle mechanical dissociation of embryonic brains with fire polished pipettes and centrifugation through sucrose gradient to separate live cell population (Bonifacino, 1998; Johansson et al., 1999).

**Cell-surface labeling, internalization and pulse-chase protein expression analyses—**Cell surface proteins were biotinylated with 1 mg/ml EZ-link sulfo-NHS-SS-biotin for 30 min at 4°C in HBSS (Gibco). The cells were washed with ice-cold HBSS containing 25mM lysine and lysed in ice-cold IP buffer: 1xPBS, 1% NP-40, 1mM EDTA, 50mM glycine, inhibitors of proteases. The resulting lysates were incubated with streptavidin beads for 2 h at 4°C and the pulled-down cell surface proteins were detected by western blotting.

For cell surface protein internalization analysis, the cells with biotinylated cell-surface proteins were incubated for indicated time in NSC growth media at 37°C. The remaining cell surface biotin was stripped by two 20 min washes with ice-cold 60 mM reduced glutathione in PBS. Cell were rinsed with ice-cold HBSS, incubated once for 5 min in solution of 5 mg/ml iodoacetamide in HBSS to quench any residual gluthathione, and rinsed twice with ice-cold HBSS. Cells were lysed in ice-cold IP buffer and the biotinylated internalized proteins were detected by pull-down with streptavidin beads and western blotting, as described above.

For pulse-chase protein analysis, the newly synthesized in ENSCs proteins were labeled by 15 min pulse of EXPRE$^{35}$S$^{35}$S Protein Labeling Mix and chased for indicated time in media with excess unlabeled methionine and cysteine. Cell surface proteins were biotinylated on ice and cells were lysed in ice-cold IP buffer. N-cadherin was first immunoprecipitated with anti-N-cadherin antibodies and protein-A/G-agarose. Bound to beads total N-cadherin was released by boiling for 2 min in 100 μl 0.5% SDS in PBS. The eluates were diluted 1:10 with ice-cold IP buffer and cell-surface N-cadherin was pulled down with streptavidin beads. Samples of total and cell-surface N-cadherin were separated on PAGE and resulting gels were incubated in Amplify for 30 min, dried and exposed for 2–4 months at -80°C with Kodak BioMAX intensifying screen and film to detect [S35]-labeled proteins.

**Statistical Analysis—**The two-tailed Student's t-test was used to calculate P values. Graphs display mean values +/− standard deviation.

## Supplementary Material

Refer to Web version on PubMed Central for supplementary material.

## Acknowledgments

This work was partially supported by the FHCRC bridge funds, NIH grants CA131047, NS080194, CA179914 and 5T32HD007183. YJ is supported by the Belgian National Funds for Scientific Research (FNRS).

## References

Betschinger J, Eisenhaber F, Knoblich JA. Phosphorylation-Induced Autoinhibition Regulates the Cytoskeletal Protein Lethal (2) giant larvae. Curr Biol. 2005; 15:276–282. [PubMed: 15694314]

Betschinger J, Mechtler K, Knoblich JA. The Par complex directs asymmetric cell division by phosphorylating the cytoskeletal protein Lgl. Nature. 2003; 422:326–330. [PubMed: 12629552]

Bilder D, Schober M, Perrimon N. Integrated activity of PDZ protein complexes regulates epithelial polarity. Nat Cell Biol. 2003; 5:53–58. [PubMed: 12510194]

Bonifacino, JS. Current protocols in cell biology. New York: John Wiley; 1998.

Cappello S, Attardo A, Wu X, Iwasato T, Itohara S, Wilsch-Brauninger M, Eilken HM, Rieger MA, Schroeder TT, Huttner WB, et al. The Rho-GTPase cdc42 regulates neural progenitor fate at the apical surface. Nat Neurosci. 2006; 9:1099–1107. [PubMed: 16892058]

Cappello S, Bohringer CR, Bergami M, Conzelmann KK, Ghanem A, Tomassy GS, Arlotta P, Mainardi M, Allegra M, Caleo M, et al. A radial glia-specific role of RhoA in double cortex formation. Neuron. 2012; 73:911–924. [PubMed: 22405202]

Cappello S, Gray MJ, Badouel C, Lange S, Einsiedler M, Srour M, Chitayat D, Hamdan FF, Jenkins ZA, Morgan T, et al. Mutations in genes encoding the cadherin receptor-ligand pair DCHS1 and FAT4 disrupt cerebral cortical development. Nat Genet. 2013; 45:1300–1308. [PubMed: 24056717]

Carabalona A, Beguin S, Pallesi-Pocachard E, Buhler E, Pellegrino C, Arnaud K, Hubert P, Oualha M, Siffroi JP, Khantane S, et al. A glial origin for periventricular nodular heterotopia caused by impaired expression of Filamin-A. Human molecular genetics. 2012; 21:1004–1017. [PubMed: 22076441]

Chenn A, Zhang YA, Chang BT, McConnell SK. Intrinsic polarity of mammalian neuroepithelial cells. Mol Cell Neurosci. 1998; 11:183–193. [PubMed: 9675050]

Clark BS, Cui S, Miesfeld JB, Klezovitch O, Vasioukhin V, Link BA. Loss of Llgl1 in retinal neuroepithelia reveals links between apical domain size, Notch activity and neurogenesis. Development. 2012; 139:1599–1610. [PubMed: 22492354]

Dahan I, Petrov D, Cohen-Kfir E, Ravid S. The tumor suppressor Lgl1 forms discrete complexes with NMII-A and Par6alpha-aPKCzeta that are affected by Lgl1 phosphorylation. J Cell Sci. 2014; 127:295–304. [PubMed: 24213535]

Das BS, Thurnham DI, Patnaik JK, Das DB, Satpathy R, Bose TK. Increased plasma lipid peroxidation in riboflavin-deficient, malaria-infected children. Am J Clin Nutr. 1990; 51:859–863. [PubMed: 2185624]

Dollar GL, Weber U, Mlodzik M, Sokol SY. Regulation of Lethal giant larvae by Dishevelled. Nature. 2005; 437:1376–1380. [PubMed: 16251968]

Feng Y, Walsh CA. The many faces of filamin: a versatile molecular scaffold for cell motility and signalling. Nat Cell Biol. 2004; 6:1034–1038. [PubMed: 15516996]

Ferland RJ, Batiz LF, Neal J, Lian G, Bundock E, Lu J, Hsiao YC, Diamond R, Mei D, Banham AH, et al. Disruption of neural progenitors along the ventricular and subventricular zones in periventricular heterotopia. Human molecular genetics. 2009; 18:497–516. [PubMed: 18996916]

Fox JW, Lamperti ED, Eksioglu YZ, Hong SE, Feng Y, Graham DA, Scheffer IE, Dobyns WB, Hirsch BA, Radtke RA, et al. Mutations in filamin 1 prevent migration of cerebral cortical neurons in human periventricular heterotopia. Neuron. 1998; 21:1315–1325. [PubMed: 9883725]

Francis F, Meyer G, Fallet-Bianco C, Moreno S, Kappeler C, Socorro AC, Tuy FP, Beldjord C, Chelly J. Human disorders of cortical development: from past to present. Eur J Neurosci. 2006; 23:877–893. [PubMed: 16519653]

Graus-Porta D, Blaess S, Senften M, Littlewood-Evans A, Damsky C, Huang Z, Orban P, Klein R, Schittny JC, Muller U. Beta1-class integrins regulate the development of laminae and folia in the cerebral and cerebellar cortex. Neuron. 2001; 31:367–379. [PubMed: 11516395]

Harlow, E., Lane, D. Using antibodies : a laboratory manual. Cold Spring Harbor, N.Y: Cold Spring Harbor Laboratory Press; 1999.

Imai F, Hirai S, Akimoto K, Koyama H, Miyata T, Ogawa M, Noguchi S, Sasaoka T, Noda T, Ohno S. Inactivation of aPKC{lambda} results in the loss of adherens junctions in neuroepithelial cells without affecting neurogenesis in mouse neocortex. Development. 2006; 133:1735–1744. [PubMed: 16571631]

Johansson CB, Momma S, Clarke DL, Risling M, Lendahl U, Frisen J. Identification of a neural stem cell in the adult mammalian central nervous system. Cell. 1999; 96:25–34. [PubMed: 9989494]

Jossin Y, Cooper JA. Reelin, Rap1 and N-cadherin orient the migration of multipolar neurons in the developing neocortex. Nat Neurosci. 2011; 14:697–703. [PubMed: 21516100]

Jossin Y, Goffinet AM. Reelin signals through phosphatidylinositol 3-kinase and Akt to control cortical development and through mTor to regulate dendritic growth. Mol Cell Biol. 2007; 27:7113–7124. [PubMed: 17698586]

Jossin Y, Ogawa M, Metin C, Tissir F, Goffinet AM. Inhibition of SRC family kinases and non-classical protein kinases C induce a reeler-like malformation of cortical plate development. J Neurosci. 2003; 23:9953–9959. [PubMed: 14586026]

Junghans D, Hack I, Frotscher M, Taylor V, Kemler R. Beta-catenin-mediated cell-adhesion is vital for embryonic forebrain development. Dev Dyn. 2005; 233:528–539. [PubMed: 15844200]

Kadowaki M, Nakamura S, Machon O, Krauss S, Radice GL, Takeichi M. N-cadherin mediates cortical organization in the mouse brain. Dev Biol. 2007; 304:22–33. [PubMed: 17222817]

Katayama K, Melendez J, Baumann JM, Leslie JR, Chauhan BK, Nemkul N, Lang RA, Kuan CY, Zheng Y, Yoshida Y. Loss of RhoA in neural progenitor cells causes the disruption of adherens

junctions and hyperproliferation. Proc Natl Acad Sci U S A. 2011; 108:7607–7612. [PubMed: 21502507]

Kim S, Lehtinen MK, Sessa A, Zappaterra MW, Cho SH, Gonzalez D, Boggan B, Austin CA, Wijnholds J, Gambello MJ, et al. The apical complex couples cell fate and cell survival to cerebral cortical development. Neuron. 2010; 66:69–84. [PubMed: 20399730]

Klezovitch O, Fernandez TE, Tapscott SJ, Vasioukhin V. Loss of cell polarity causes severe brain dysplasia in Lgl1 knockout mice. Genes Dev. 2004; 18:559–571. [PubMed: 15037549]

Laprise P, Viel A, Rivard N. Human homolog of disc-large is required for adherens junction assembly and differentiation of human intestinal epithelial cells. J Biol Chem. 2004; 279:10157–10166. [PubMed: 14699157]

Lian G, Sheen VL. Cytoskeletal proteins in cortical development and disease: actin associated proteins in periventricular heterotopia. Front Cell Neurosci. 2015; 9:99. [PubMed: 25883548]

Lien WH, Gelfand VI, Vasioukhin V. Alpha-E-catenin binds to dynamitin and regulates dynactin-mediated intracellular traffic. J Cell Biol. 2008; 183:989–997. [PubMed: 19075109]

Lien WH, Klezovitch O, Fernandez TE, Delrow J, Vasioukhin V. alphaE-catenin controls cerebral cortical size by regulating the hedgehog signaling pathway. Science. 2006; 311:1609–1612. [PubMed: 16543460]

Lu J, Sheen V. Periventricular heterotopia. Epilepsy Behav. 2005; 7:143–149. [PubMed: 15996530]

Ma X, Bao J, Adelstein RS. Loss of cell adhesion causes hydrocephalus in nonmuscle myosin II-B-ablated and mutated mice. Mol Biol Cell. 2007; 18:2305–2312. [PubMed: 17429076]

Machon O, van den Bout CJ, Backman M, Kemler R, Krauss S. Role of beta-catenin in the developing cortical and hippocampal neuroepithelium. Neuroscience. 2003; 122:129–143. [PubMed: 14596855]

Manabe N, Hirai S, Imai F, Nakanishi H, Takai Y, Ohno S. Association of ASIP/mPAR-3 with adherens junctions of mouse neuroepithelial cells. Dev Dyn. 2002; 225:61–69. [PubMed: 12203721]

Mochida GH, Walsh CA. Genetic basis of developmental malformations of the cerebral cortex. Arch Neurol. 2004; 61:637–640. [PubMed: 15148137]

Plant PJ, Fawcett JP, Lin DC, Holdorf AD, Binns K, Kulkarni S, Pawson T. A polarity complex of mPar-6 and atypical PKC binds, phosphorylates and regulates mammalian Lgl. Nat Cell Biol. 2003; 5:301–308. [PubMed: 12629547]

Prehoda KE. Polarization of Drosophila neuroblasts during asymmetric division. Cold Spring Harb Perspect Biol. 2009; 1:a001388. [PubMed: 20066083]

Qin Y, Capaldo C, Gumbiner BM, Macara IG. The mammalian Scribble polarity protein regulates epithelial cell adhesion and migration through E-cadherin. J Cell Biol. 2005; 171:1061–1071. [PubMed: 16344308]

Raman R, Damle I, Rote R, Banerjee S, Dingare C, Sonawane M. aPKC regulates apical localization of Lgl to restrict elongation of microridges in developing zebrafish epidermis. Nature communications. 2016; 7:11643.

Saito T. In vivo electroporation in the embryonic mouse central nervous system. Nat Protoc. 2006; 1:1552–1558. [PubMed: 17406448]

Schmid MT, Weinandy F, Wilsch-Brauninger M, Huttner WB, Cappello S, Gotz M. The role of alpha-E-catenin in cerebral cortex development: radial glia specific effect on neuronal migration. Front Cell Neurosci. 2014; 8:215. [PubMed: 25147501]

Sheen VL, Ganesh VS, Topcu M, Sebire G, Bodell A, Hill RS, Grant PE, Shugart YY, Imitola J, Khoury SJ, et al. Mutations in ARFGEF2 implicate vesicle trafficking in neural progenitor proliferation and migration in the human cerebral cortex. Nat Genet. 2004; 36:69–76. [PubMed: 14647276]

Smutny M, Cox HL, Leerberg JM, Kovacs EM, Conti MA, Ferguson C, Hamilton NA, Parton RG, Adelstein RS, Yap AS. Myosin II isoforms identify distinct functional modules that support integrity of the epithelial zonula adherens. Nat Cell Biol. 2010; 12:696–702. [PubMed: 20543839]

Spear PC, Erickson CA. Interkinetic nuclear migration: a mysterious process in search of a function. Dev Growth Differ. 2012; 54:306–316. [PubMed: 22524603]

Sripathy S, Lee M, Vasioukhin V. Mammalian Llgl2 is necessary for proper branching morphogenesis during placental development. Molecular and cellular biology. 2011; 31:2920–2933. [PubMed: 21606200]

Strand D, Unger S, Corvi R, Hartenstein K, Schenkel H, Kalmes A, Merdes G, Neumann B, Krieg-Schneider F, Coy JF, et al. A human homologue of the Drosophila tumour suppressor gene l(2)gl maps to 17p11.2–12 and codes for a cytoskeletal protein that associates with nonmuscle myosin II heavy chain. Oncogene. 1995; 11:291–301. [PubMed: 7542763]

Tabata H, Nakajima K. Efficient in utero gene transfer system to the developing mouse brain using electroporation: visualization of neuronal migration in the developing cortex. Neuroscience. 2001; 103:865–872. [PubMed: 11301197]

Tanentzapf G, Tepass U. Interactions between the crumbs, lethal giant larvae and bazooka pathways in epithelial polarization. Nat Cell Biol. 2003; 5:46–52. [PubMed: 12510193]

Teng J, Rai T, Tanaka Y, Takei Y, Nakata T, Hirasawa M, Kulkarni AB, Hirokawa N. The KIF3 motor transports N-cadherin and organizes the developing neuroepithelium. Nat Cell Biol. 2005; 7:474–482. [PubMed: 15834408]

Tronche F, Kellendonk C, Kretz O, Gass P, Anlag K, Orban PC, Bock R, Klein R, Schutz G. Disruption of the glucocorticoid receptor gene in the nervous system results in reduced anxiety. Nat Genet. 1999; 23:99–103. [PubMed: 10471508]

Vasioukhin V. Lethal giant puzzle of lgl. Dev Neurosci. 2006; 28:13–24. [PubMed: 16508300]

Yamanaka T, Horikoshi Y, Sugiyama Y, Ishiyama C, Suzuki A, Hirose T, Iwamatsu A, Shinohara A, Ohno S. Mammalian Lgl forms a protein complex with PAR-6 and aPKC independently of PAR-3 to regulate epithelial cell polarity. Curr Biol. 2003; 13:734–743. [PubMed: 12725730]

Yap AS, Gomez GA, Parton RG. Adherens Junctions Revisualized: Organizing Cadherins as Nanoassemblies. Dev Cell. 2015; 35:12–20. [PubMed: 26460944]

Zechner D, Fujita Y, Hulsken J, Muller T, Walther I, Taketo MM, Crenshaw EB 3rd, Birchmeier W, Birchmeier C. beta-Catenin signals regulate cell growth and the balance between progenitor cell expansion and differentiation in the nervous system. Dev Biol. 2003; 258:406–418. [PubMed: 12798297]

## Highlights

- LLGL1 loss in embryonic neural stem cells (ENSC) results in cortical heterotopia
- LLGL1 is necessary for the maintenance of Apical Junctional complexes in ENSCs
- LLGL1 binds to and regulates cell surface levels and localization of N-cadherin
- Disruption of N-cadherin-LLGL1 interaction results in cortical heterotopia

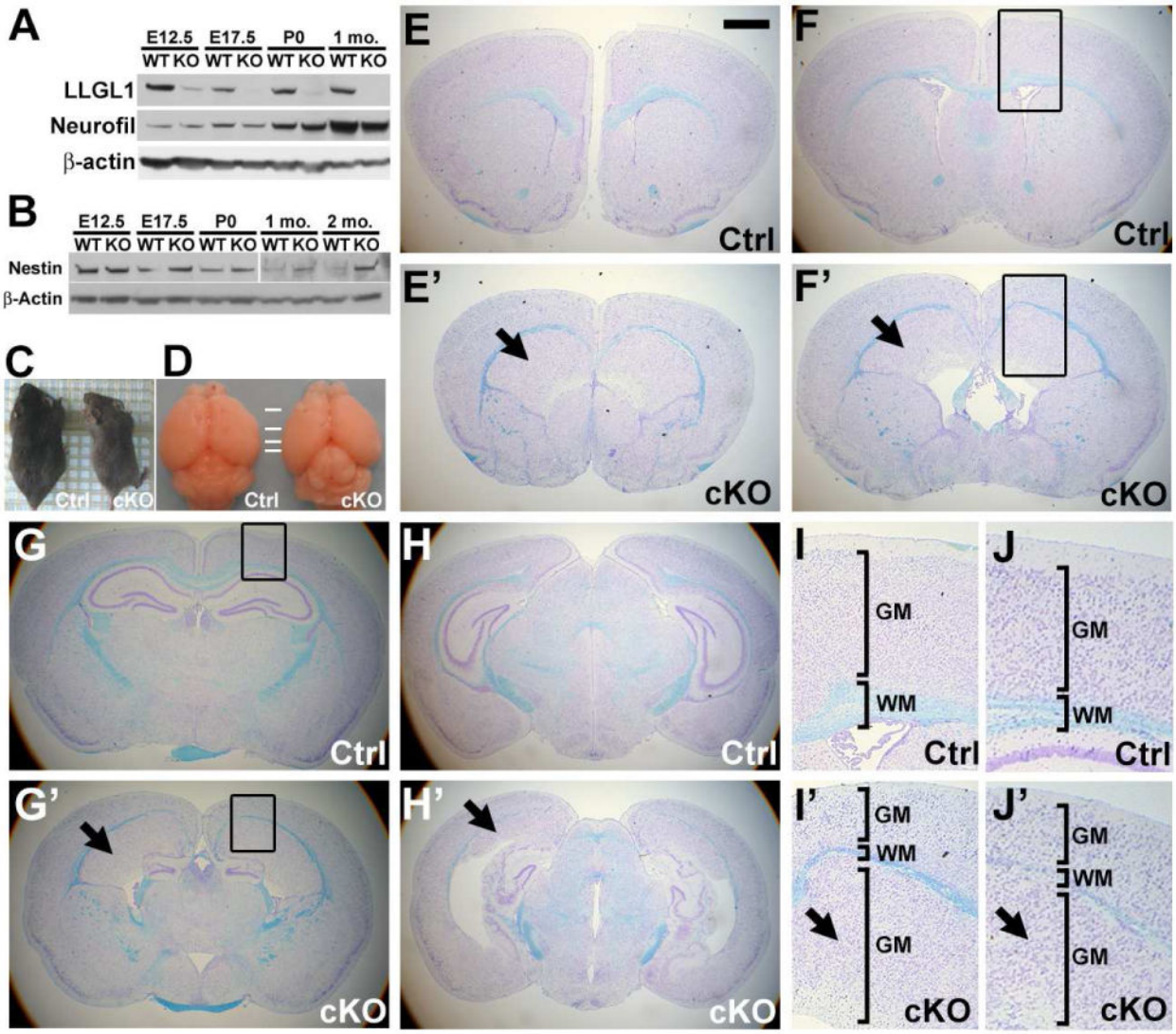


**Figure 1. Severe brain malformation in *Llgl1*$^{LoxP/LoxP}$/*Nestin-Cre*$^{+/-}$ (cKO *Llgl1*) mice**

**(A–B)** Western blot analysis of total protein extracts from E12.5, E17.5, P0, and 1 month-old (1 mo.) control (Ctrl) and cKO *Llgl1* (cKO) brains with anti-*Llgl1*, anti-Nestin, anti-Neurofilament and anti-β-actin antibodies.

**(C–D)** General appearance and brains of 2 month-old control (Ctrl) and cKO *Llgl1* (cKO) mice.

**(E–J′)** Histologic appearance of brains from 2 month-old control (Ctrl) and cKO *Llgl1* (cKO) mice. Nissl staining of coronal sections at the levels of lateral ventricles (E–F′, I–I′) and hippocampus (G–H′, J–J′). Areas in brackets in F, F′ and G, G′ are shown at higher magnification in I, I′ and J, J′, respectively. GM indicates gray matter. WM indicates white matter. Arrows indicate ectopically-formed layer of gray matter. Representative images from 5 Ctrl and 6 cKO *Llgl1* brains. Bar in E represents 830 μm in E,E′, 930 μm in F, F′, 1 mm in G,G′, 1.03 mm in H, H′, 410 μm in I,I′ and 212 μm in J,J′.

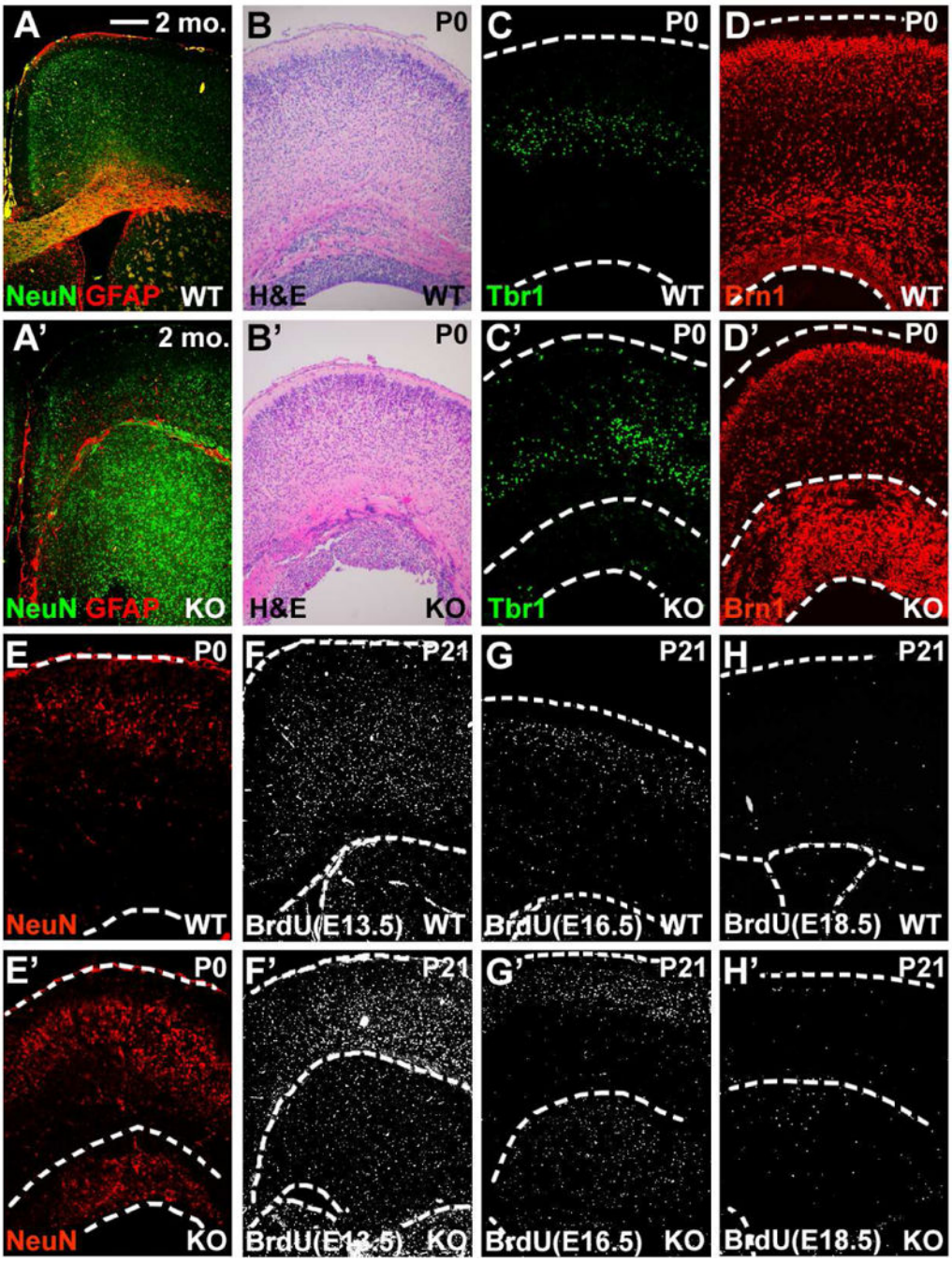


**Figure 2. Periventricular heterotopia in cKO *Llgl1* brains**

**(A–A′)** Immunostaining of coronal cerebral cortical sections from 2-month-old (2 mo.) control (Ctrl) and cKO *Llgl1* (cKO) brains with anti-NeuroN (NeuN) and anti-GFAP antibodies. Representative images from 2 Ctrl and 3 cKO *Llgl1* brains.

**(B–E′)** Stainings of coronal cortical sections from newborn (P0) control (Ctrl) and cKO *Llgl1* (cKO) brains with hematoxylin and eosin (B, B′), or with anti-Tbr1 (C, C′), anti-Brn1 (D, D′) and anti-NeuroN (NeuN, E, E′) antibodies. Representative images from 6 Ctrl and 4 cKO *Llgl1* brains.

**(F–H)** BrdU birthdating of cells in control (Ctrl) and cKO *Llgl1* (cKO) cortexes. BrdU was injected at E13.5 (F, F′, 4 Ctrl and 3 cKO mice), E16.5 (G, G′, 5 Ctrl and 5 cKO mice), E18.5 (H, H′, 3 Ctrl and 3 cKO mice). Cells that incorporated BrdU at the time of injection were revealed by immunostaining with anti-BrdU antibodies 21 days after birth (P21). Dashed lines in C–H′ indicate boundaries of the cortex. The additional dashed line in the middle of the cortex in the KO panels indicates the location of the white matter separating the cerebral cortical plate and ectopic neuronal layer at the ventricular surface. Bar in A represents 265 μm in A, A′, F–H′, 125 μm in B–B′, and 105 μm in C–E′. See also Figure S1.

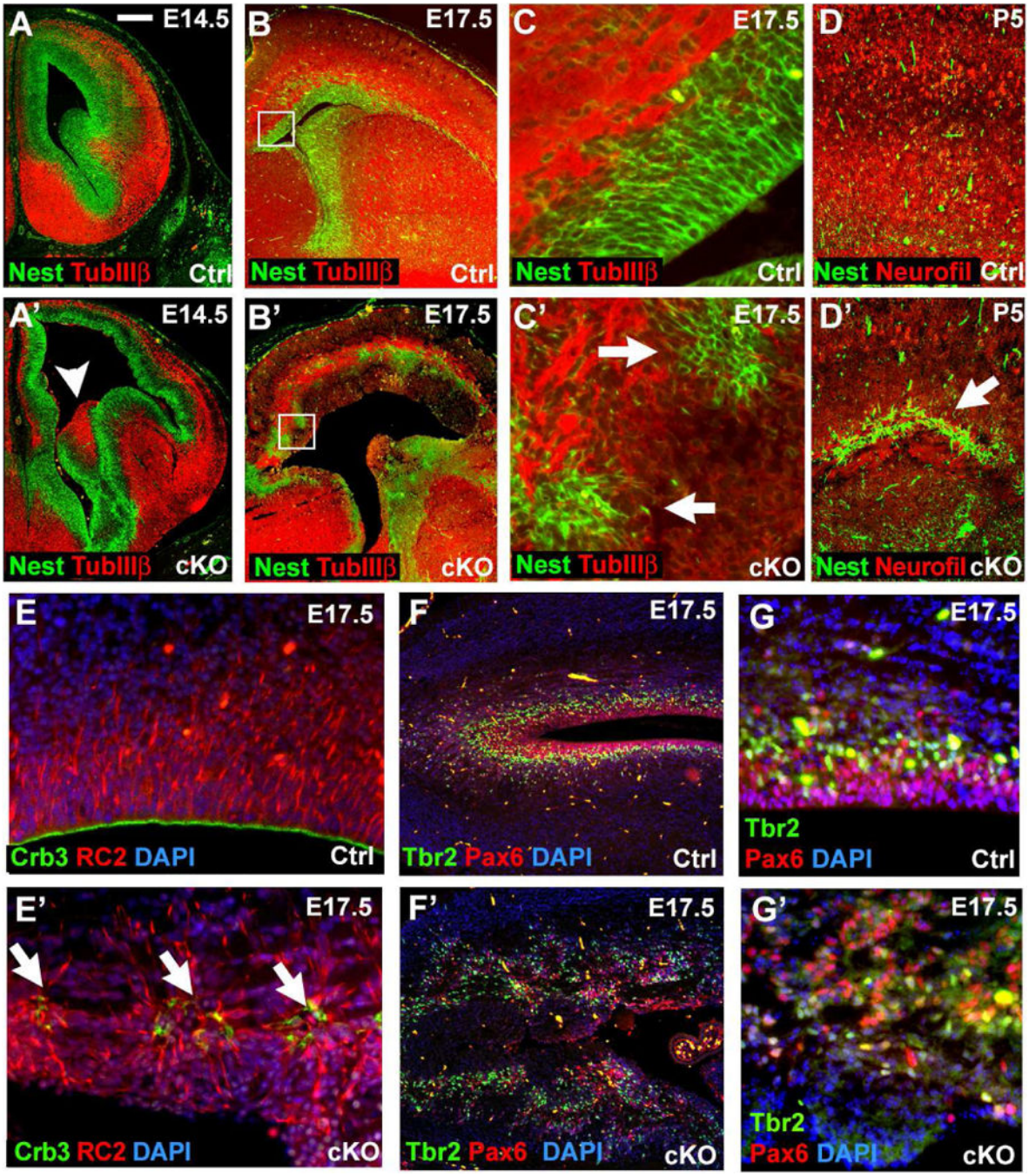


**Figure 3. Dynamics of periventricular heterotopia in cKO *Llgl1* brains**

**(A–C′)** Immunostainings of coronal brain sections at the level of the lateral ventricle from E14.5 (A–A′) and E17.5 (B–C′) control (Ctrl) and cKO *Llgl1* (cKO) brains with anti-Nestin (Nest, ENSC marker, green), anti-β-Tubulin III (TubIIIβ, early neuronal marker, red) antibodies. Areas boxed in B, B′ are shown at higher magnification in C, C′, respectively. Representative images from 3 Ctrl and 3 cKO *Llgl1* brains. Arrows indicate misplaced ENSCs.

**(D–D′)** Immunostainings of coronal brain sections at the level of the lateral ventricle from 5 day-old (P5) control (Ctrl) and cKO *Llgl1* (cKO) brains with anti-Nestin (green) and anti-Neurofilament (red) antibodies. Representative images from 2 Ctrl and 3 cKO *Llgl1* brains. Arrow indicates a layer of ENSCs in the middle of cKO cortex.

**(E–G′)** Immunostainings of coronal brain sections from E17.5 control (Ctrl) and cKO *Llgl1* (cKO) brains with anti-RC2 (radial glial marker, red in E–E′), anti-Crumbs3 (Crb3, apical membrane domain marker, green in E–E′), anti-Pax6 (VZ ENSC marker, red in F–G′) and anti-Tbr2 (SVZ progenitor marker, green in F–G′). Representative images from 3 Ctrl and 3 cKO *Llgl1* brains. Arrows indicate neuroepithelial rosettes in cKO *Llgl1* brains. Bar in A represents 260 μm in A–A′, 210 μm in B–B′, 21 μm in C–C′ 105 μm in D–D′, 20 μm in E–E′, G–G′, and 80 μm in F–F′. See also Figure S2.

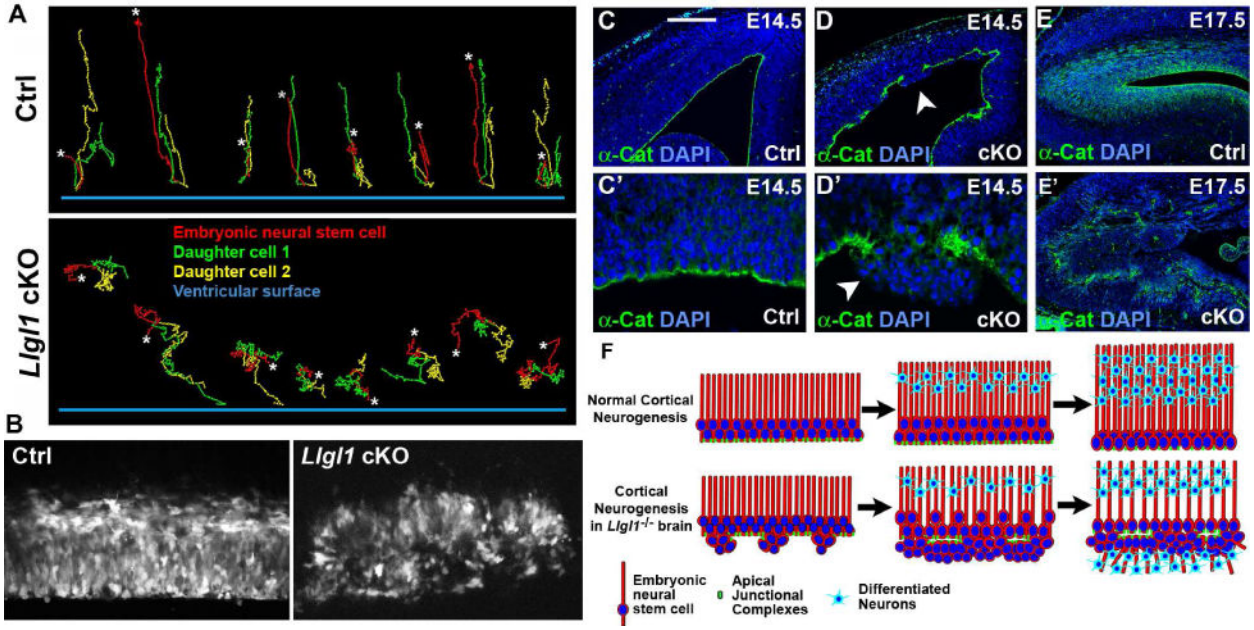


**Figure 4. In vivo time-lapse imaging and immunostaining analyses reveal disruption of AJCs and internalization of ENSCs in cKO *Llgl1* brains**

**(A)** Nuclear tracks of ENSCs and their daughters in the ventricular zone of control (Ctrl) and cKO *Llgl1* (cKO) brains from Supplementary Video 5. Brains were electroporated with NLS-GFP expressing vector at E12.5 and cortical slices were prepared and imaged at E13.5. n=2 for Ctrl and n=2 for cKO *Llgl1*. Note, in control cortexes, nuclei of ENSCs (in red) move towards the ventricular surface (blue line) to divide. The two daughter cells (green and yellow) then move away from the ventricular surface. In contrast, cKO *Llgl1* ENSCs show random movements and divide at a distance from the ventricular surface. Asterisks show the initial position of tracked cells.

**(B)** Neuroepithelial rosettes in cKO *Llgl1* (cKO) brains. Still image from Supplementary Video 6. Brains were electroporated with NLS-GFP expressing vector at E14.5 and cortical slices were prepared and imaged at E16.5. n=2 for Ctrl and n=2 for cKO *Llgl1*.

**(C–E′)** Coronal brain sections from E14.5 and E17.5 control (Ctrl) and cKO *Llgl1* (cKO) brains were stained with anti-α-Catenin (α-Cat, AJC marker, green) antibodies. Note protrusion of cortical cells in the areas with disrupted AJCs in E14.5 cKO *Llgl1* brains (white arrowheads), and complete internalization of AJCs in E17.5 mutants. Representative images from 3 Ctrl and 3 cKO *Llgl1* brains.

**(F)** Model of PH formation in cKO *Llgl1* brains. ENSCs display focal loss of AJCs. Cortical cells protrude into the ventricle and expand on the apical membrane domains of polarized ENSCs. ENSCs are engulfed by nonpolarized neighbors and are misplaced inside the developing cortex. Misplaced ENSCs send neurons towards both the developing cortical plate and the ventricle, creating an ectopic neuronal layer at the ventricular surface. Bar in C represents 210 μm in C, D, E, E′; 70 μm in C′, D′. See also Figure S3.

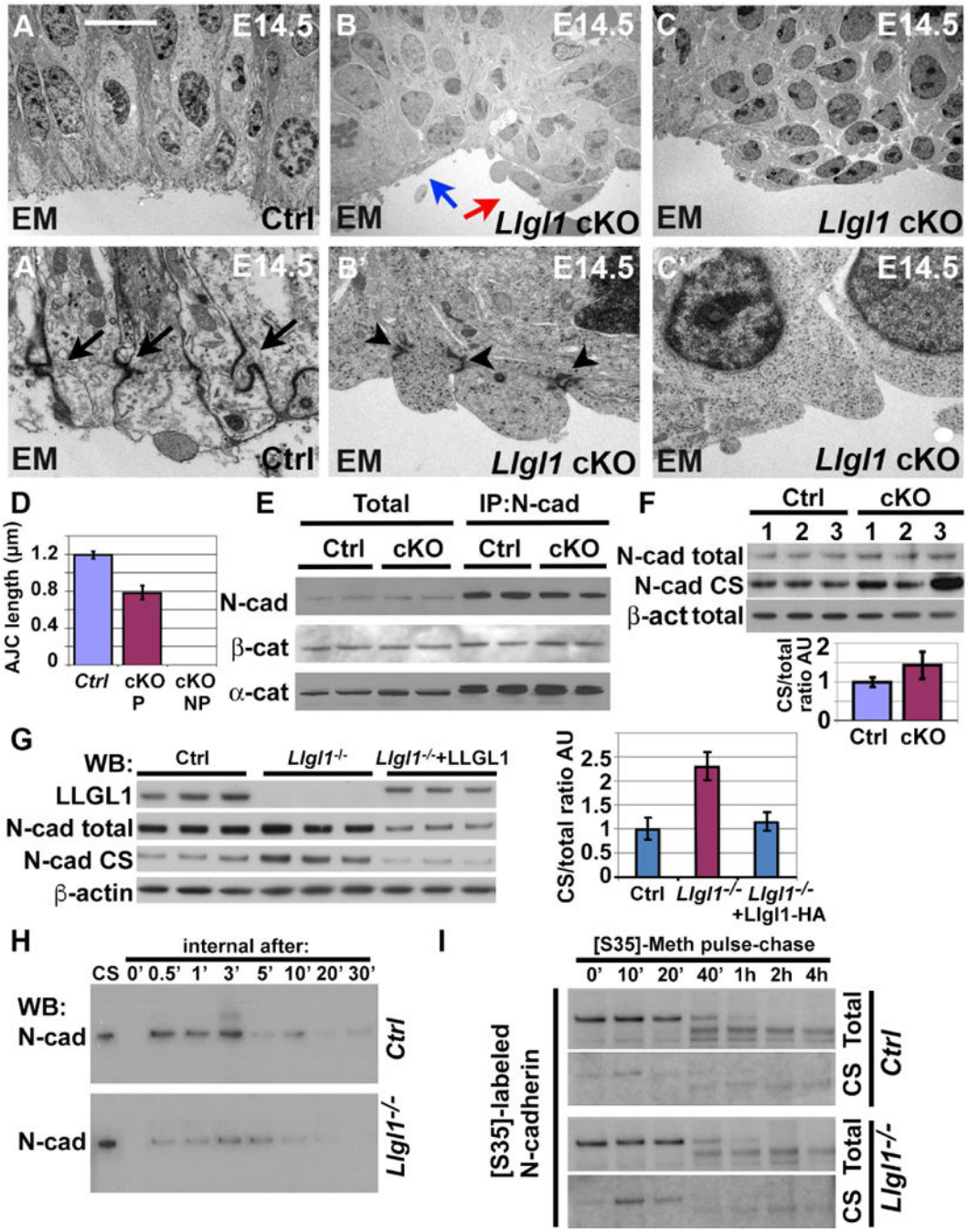


**Figure 5. LLGL1 is necessary for the maintenance of AJCs in ENSCs**

**(A–C′)** Electron microscopy analysis of cortical sections from E14.5 wild-type (WT) and *Llgl1* cKO (KO) embryos. Self-renewing WT VZ ENSCs display prominent AJCs (A–A′). Black arrows indicate AJCs. Frame B shows the boundary between properly polarized adhesive ENSCs (blue arrow) and the cells protruding into the ventricle (red arrow). Polarized *Llgl1* cKO VZ ENSCs display small AJCs (black arrowheads in B′). Representative images from the analyses of 3 Ctrl and 3 *Llgl1* cKO brains. Frames C–C′

show the area containing protruding into the ventricle ENSCs lacking AJCs. Bar in A represents 9 μm in A, B, C and 1.5 μm in A′, B′, C′.

**(D)** Quantitation of the lengths of AJCs in control (Ctrl) and polarized (P) and non-polarized (NP) *Llgl1* cKO (cKO) ENSCs. Data from 3 Ctrl and 3 *Llgl1* cKO brains. n=102 for Ctrl, n=71 for *Llgl1* cKO. Graph shows mean values +/− SD.

**(E)** Normal cadherin/catenin complex formation in *Llgl1* cKO brains. Total protein lysates from E14.5 two Ctrl and two *Llgl1* cKO brains were immunoprecipitated with anti-N-cadherin antibodies and analyzed by Western blotting with anti-N-Cadherin, anti-β-catenin and anti-α-catenin antibodies.

**(F)** Cell-surface (CS) levels of N-cadherin in E14.5 3 control (Ctrl) and 3 *Llgl1* cKO ENSCs. Cell surface proteins on isolated ENSCs were biotinylated, precipitated with streptavidin-sepharose and blotted with anti-N-cadherin antibodies. Quantitation of CS to total levels of N-cadherin. Graph shows mean values +/− SD. Ratio of surface to total levels of N-cadherin in control (Ctrl) cells is arbitrary adjusted to 1.

**(G)** Cell-surface (CS) levels of N-cadherin in cultured 3 control (Ctrl), 3 $Llgl1^{-/-}$ and 3 rescued by re-expression of LLGL1 in $Llgl1^{-/-}$ cells ($Llgl1^{-/-}$ +LLGL1) ENSCs cultures. Graph shows mean values +/− SD.

**(H)** Internalization of cell-surface N-cadherin in cultured control (Ctrl) and $Llgl1^{-/-}$ ENSCs. Cell surface proteins were biotinylated, incubated at 37°C for indicated number of min, stripped with reduced glutathione, precipitated with streptavidin-sepharose and blotted with anti-N-cadherin antibodies. CS–total levels of cell-surface N-cadherin. Representative data from 3 independent experiments.

**(I)** Cell surface delivery and retention of N-cadherin in cultured control (Ctrl) and $Llgl1^{-/-}$ENSCs. Newly synthesized proteins were labeled by pulse of [S35]Met/Cys and chased for indicated time. Proteins immunoprecipitated with anti-N-cadherin antibodies, released from the beads (total new N-cadherin), and then re-precipitated by streptavidin-sepharose (cell surface, CS, new N-cadherin). Representative data from 3 independent experiments. See also Figure S4.

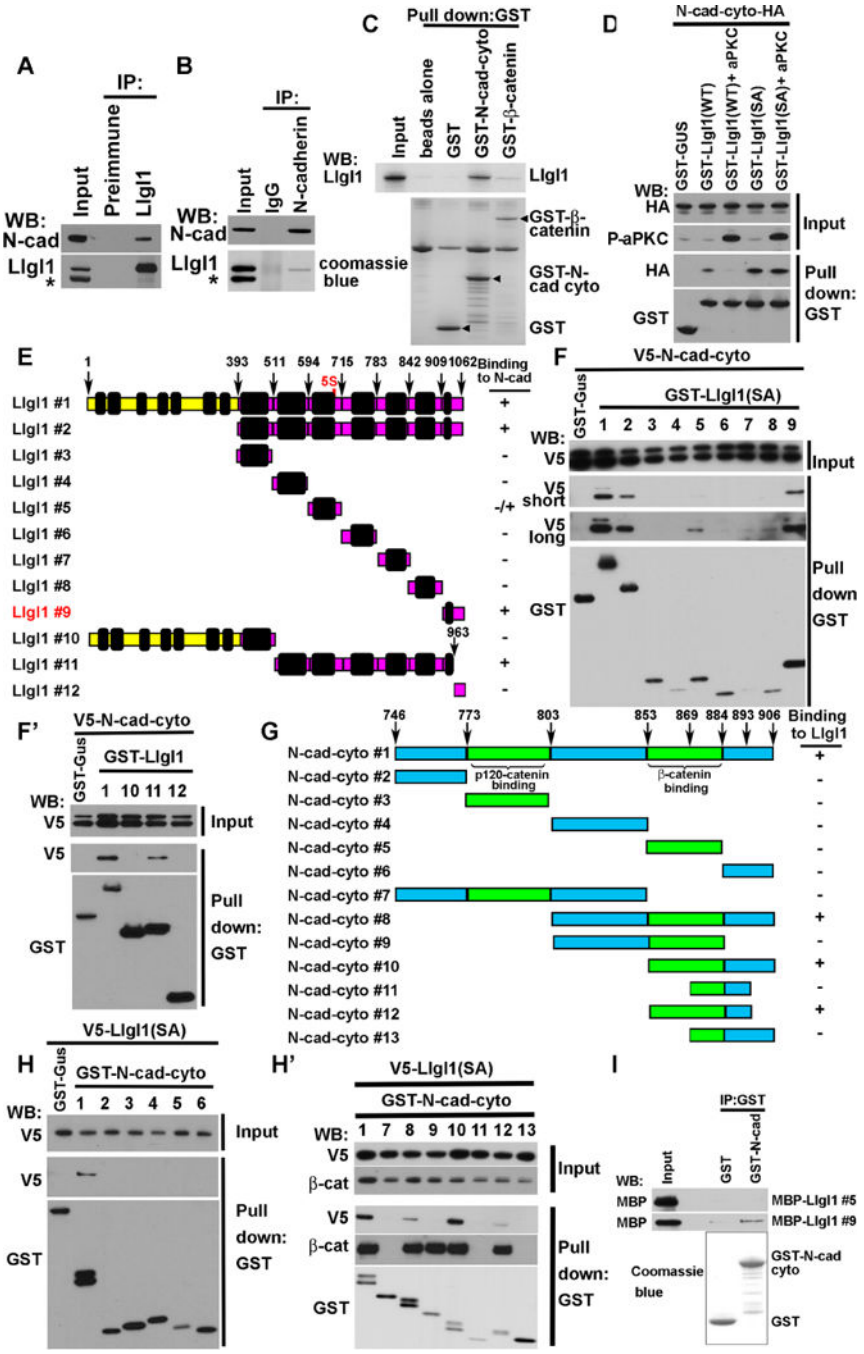


**Figure 6. Physical interaction between N-cadherin and Llgl1**

**(A–B)** Co-immunoprecipitation between endogenous N-cadherin and Llgl1 in embryonic brains. Western blot (WB:) analyses of total (Input) and immunoprecipitated using control preimmune, anti-Llgl1 or anti-N-cadherin antibodies proteins with anti-N-cadherin and anti-Llgl1 antibodies. Representative data from 2 independent experiments for A and 3 independent experiments for B. Asterisks indicate non-specific band.

**(C)** Western blot (WB:) analysis and coomassie staining of total (Input) and pulled-down using beads-alone, GST, GST-N-cadherin cytoplasmic domain (N-cad-cyto), and GST-β-catenin embryonic brain proteins. Representative data from 2 independent experiments.
**(D)** Western blot (WB:) analyses of total (Input) and GST-pull-down using control GST-GUS, GST-LLGL1 wild-type (LLGL1 WT) and GST-LLGL1 five SA mutant (LLGL1 SA) proteins extracted from HEK293 cells transfected with HA-tagged N-cadherin cytoplasmic domain (N-cad-cyto-HA) and constitutively-active aPKC (aPKC) expression constructs. Representative data from 3 independent experiments.
**(E)** Diagram of LLGL1 fragment/deletion constructs used to identify N-cadherin binding domain. WD domains 1–14 are shown in black.
**(F–F′)** C-terminal domain of LLGL1 binds to N-cadherin. Western blot (WB) analyses of pulled-down with glutathione-sepharose proteins extracted from HEK293 cells expressing V5-tagged N-cadherin cytoplasmic domain (V5-N-cad cyto) and indicated GST-tagged fragments of LLGL1. V5-short and V5-long indicate shorter and longer exposure. Representative data from 2 independent experiments.
**(G)** Diagram showing N-cadherin cytoplasmic domain fragments/deletion constructs used to identify LLGL1 binding domain.
**(H–H′)** Region containing amino acids 853–893 of murine N-cadherin binds to LLGL1, which is not phosphorylated by aPKC. Western blot (WB) analyses of pulled-down with glutathione-sepharose proteins extracted from HEK293 cells expressing V5-tagged LLGL1(SA) mutant and indicated GST-tagged fragments of N-cadherin. Representative data from 2 independent experiments.
**(I)** Direct interaction between LLGL1 and N-cadherin. Western blot (WB) analysis and coomassie staining of inputs and pulled-down with GST or GST-N-cadherin cytoplasmic domain (IP:GST) MBP-tagged LLGL1#5 and #9 proteins (see frame E). Representative data from 2 independent experiments. See also Figure S5.

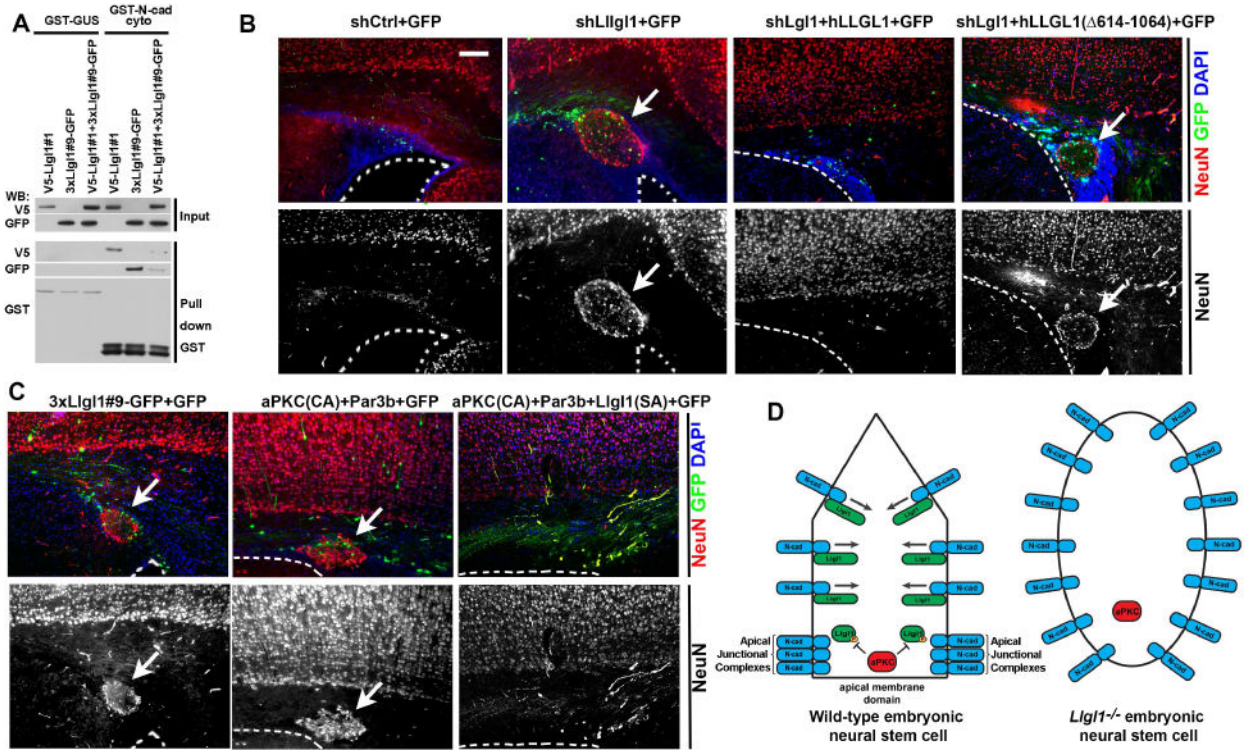


**Figure 7. In vivo disruption of interaction between LLGL1 and N-cadherin during brain development results in formation of PH**

**(A)** Multimerized LLGL1 fragment #9 weakens interaction between N-cadherin and LLGL1. Western blot (WB) analyses of total protein extracts (Input) or pulled-down with glutathione-sepharose proteins extracted from HEK293 cells expressing triple tandem repeat of LLGL1 #9 fused to GFP (3xLlgl1#9-GFP), full-length V5-tagged LLGL1(SA) mutant, negative control GST-GUS and GST-N-cadherin cytoplasmic domain proteins. Representative data from 2 independent experiments.

**(B–C)** Expression of shLlgl1, membrane-targeted constitutively–active aPKC or multimerized LLGL1 fragment #9 in the developing cerebral cortex results in neuronal heterotopia. Immunostainings of coronal brain sections (at the level of the lateral ventricle) from P7 wild-type pups that were in utero electroporated at E15.5 with GFP encoding plasmid and negative control shRNA (shCtrl, 0 brains with heterotopia out of 6 electroporated brains), shLlgl1 (3 brains with heterotopia out of 3 electroporated brains), shLlgl1 +human LLGL1 (0 brains with heterotopia out of 3 electroporated brains), shLlgl1 +human LLGL1Δ614-1064 (3 brains with heterotopia out of 4 electroporated brains), aPKC +PAR3 (3 brains with heterotopia out of 3 electroporated brains), aPKC+Par3 + SA-LLGL1 (3 complete rescues out of 5 electroporated brains), or triple tandem repeat of LLGL1 #9 fused to GFP (3xLlgl1#9-GFP, 4 brains with heterotopia out of 7 electroporated brains). Red-neuronal cell marker NeuroN (NeuN). Green-GFP. Blue-DAPI. Note GFP-positive ectopic neuronal nodules in cortexes expressing shLlgl1, CA-aPKC+PAR3 and 3xLlgl1#9-GFP (arrows). White dotted lines indicate position of the ventricular surface. Bar in B represents 105 μm in B–C.

**(D)** Hypothetical model of LLGL1 function in AJC maintenance. Non-phosphorylated by aPKC LLGL1 binds to N-cadherin and promotes its internalization at the basolateral membrane domain. aPKC-mediated phosphorylation prevents LLGL1-N-cadherin interaction and promotes accumulation of N-cadherin at the interface between basolateral and apical membrane domains. See also Figure S6.